Journal of Power Sources 192 (2009) 668–673

Contents lists available at ScienceDirect

Journal of Power Sources

journal homepage: www.elsevier.com/locate/jpowsour

Synthesis and electrochemical properties of single-crystalline LiV_3O_8 nanorods as cathode materials for rechargeable lithium batteries

Haimei Liu, Yonggang Wang, Kaixue Wang, Yarong Wang, Haoshen Zhou*

Institute of Energy Technology, National Institute of Advanced Industrial Science and Technology (AIST), AIST Tsukuba Center, Umezono 1-1-1, Tsukuba, Ibaraki 305-8568, Japan

ARTICLE INFO

Article history:
Received 13 January 2009
Received in revised form 18 March 2009
Accepted 31 March 2009
Available online 8 April 2009

Keywords:
Rechargeable lithium batteries
Cathode materials
LiV_3O_8
Single-crystalline nanorods
Electrochemical measurements
Stability

ABSTRACT

One-dimensional (1D) nanorods of LiV_3O_8 single crystals have been fabricated by using well-defined home-made VO_2 (B) nanorods as the vanadium resource, combined with a convenient solid-state reaction. The as-obtained LiV_3O_8 nanorods were characterized by XRD, TEM and SEM, indicating this material was highly crystalline and a single phase. The electrochemical performance of LiV_3O_8 nanorods as the positive electrode material for rechargeable lithium batteries was investigated, which demonstrated that as-prepared LiV_3O_8 nanorods exhibited as high as 348 mAh g^{-1} discharge capacity in first cycle at 20 mA g^{-1} current density, and still remained at 303 mAh g^{-1} at 50 mA g^{-1} afterwards; moreover, until 50 cycles, they kept 315 mAh g^{-1}, recorded at 50 mA g^{-1}. All these results imply that single-crystalline 1D nanorods of LiV_3O_8 are promising cathode material for rechargeable lithium batteries.

1. Introduction

LiV_3O_8, a layered trivanadate, is a very interesting cathode material for rechargeable lithium batteries [1,2]. Since it was reported by Besenhard and Schöllhorn as an intercalation material in 30 years ago [3], considerable efforts have been devoted to studying its preparation methods, morphologies and electrochemical properties [4–7]. It should be noted that the preparation methods as well as the materials morphology can strongly influence the electrochemical performance of the electrode material LiV_3O_8, such as charge–discharge capacity, rate capacity, and cyclability [1,5], etc. In fact, up to now, many methodologies have been developed to prepare LiV_3O_8 with an aim to improve its electrochemical performance, for example, sol–gel method, rapid cooling, efficient grinding, hydrothermal method, and so on [8–10]. However, the reported rate capacity and cycling properties in all these works, were still far from its optimal target performance, thereby, it is interesting to synthesize the LiV_3O_8 with the aim to improve its electrochemical properties.

On the other hand, nano-scaled and well-ordered structures with various morphologies of lithium intercalated materials have been extensively studied, for instance, nanowires (CuV_2O_6, V_2O_5, TiO_2–B) [11–13], nanotubes (V_2O_5, $LiMn_2O_4$) [14,15], nanorods (VO_2 (B), $LiMn_2O_4$) [16,17], nanosheets (LiV_3O_8) [18], and so on. It is generally accepted that the nano-materials provide short diffusion pathway for lithium ions insertion/extraction from host materials, together with high specific surface areas which often afford more active intercalation sites [19,20]. It is to be noted that, compared to other materials, nano-scaled LiV_3O_8 was far less studied, although some efforts have been made on fabrication of LiV_3O_8 nanowires [21], 1D linear nanosheets [18], etc. However, although in the first cycle, above-mentioned 1D arrays of LiV_3O_8 nanosheets displayed a high initial discharge capacity of 352 mAh g^{-1}, the capacity drastically decreased to 255 mAh g^{-1} after 40 cycles, recorded at the current density of 40 mA g^{-1}, which corresponded to only 72.4% of the initial capacity [18]. Thereby, it is still an interesting topic to fabricate nanostructured LiV_3O_8 materials with improved electrochemical properties.

The traditional method for preparation of LiV_3O_8 is to employ V_2O_5 or NH_4VO_3 as the vanadium precursor, and accomplished by the solid-state reaction. However, such procedures commonly give the LiV_3O_8 as a bulk material. In the present work, we describe the use of home-made VO_2 (B) nanorod for the first time as vanadium precursor combined with LiOH, a novel LiV_3O_8 nanorods single-crystalline was fabricated and characterized. When used as the cathode material in rechargeable lithium batteries, the as-prepared single-crystalline LiV_3O_8 nanorods exhibited good discharge capacity, rate capacity and cycling performance.

* Corresponding author. Tel.: +81 29 861 5795; fax: +81 29 861 5799.
E-mail address: hs.zhou@aist.go.jp (H. Zhou).

0378-7753/$ – see front matter © 2009 Elsevier B.V. All rights reserved.
doi:10.1016/j.jpowsour.2009.03.066

2. Experimental

VO_2 (B) nanorods precursor was prepared by a hydrothermal method. In a typical synthesis, V_2O_5 powder (0.365 g, high purity, Wako), *n*-butanol (10 mL, 99.9%, Wako), and 30 mL H_2O were mixed under vigorous magnetic stirring at room temperature and kept for 4 h, and then an orange suspension solution was obtained. The resultant mixture was then transferred to a 40 mL autoclave and kept in an oven at 180 °C for 48 h. The product was washed with anhydrous ethanol and cyclohexane several times. The produced VO_2 precursor was dried at 80 °C in vacuum for 12 h. The crystalline VO_2 (B) nanorods were obtained by annealing the dried VO_2 precursor at 250 °C for 10 h under vacuum.

The LiV_3O_8 nanorods were prepared as following: above-obtained crystalline VO_2 (B) precursor and $LiOH{\cdot}H_2O$ (V/Li = 3/1.05, mol mol^{-1}) was mixed in methanol under magnetic stirring and kept for 12 h. The mixture solution was heated to 50 °C to evaporate the methanol. The powder mixture produced was firstly heat-treated at 150 °C for 10 h in vacuum, and finally annealed at 450 °C for 10 h in air. A brown powder sample was thus obtained. Powder X-ray diffraction (XRD) data for the synthesized materials were collected with a Bruker D8 Advanced diffractometer using Cu Kα (λ = 1.5406 Å) radiation. The Brunauer–Emmett–Teller (BET) specific surface area measurement of the product was performed on Belsorp 18 through nitrogen adsorption–desorption method, after degassing the powder sample at 150 °C for 8 h in vacuum. SEM and TEM images were taken on LEO Gemini Supra 35 and Hitachi 800 instruments, respectively.

The electrochemical performance of the synthesized LiV_3O_8 sample was measured with a beaker-type three-electrode cell. The working electrode (WE) was composed of 80% LiV_3O_8, 15% acetylene black, and 5% polytetrafluoroethylene (PTFE) binder by weight. The above mixture was spread and pressed onto a titanium mesh (100 mesh) which served as a current collector. The reference electrode (RE) and counter electrode (CE) were prepared by spreading and pressing lithium metal onto the similar titanium mesh. The electrolyte was 1 M $LiClO_4$ in ethyl carbonate (EC) and diethyl carbonate (DEC) (EC/DEC = 1:1, v/v). The cell was assembled in a glove box filled with pure argon gas. Galvanostatic discharge/charge measurements were performed in a potential range of 4.5–1.5 V vs. Li/Li^+. The specific capacity and current density were based on the weight of the active material (LiV_3O_8) only.

3. Results and discussion

The prepared VO_2 (B) precursor was firstly characterized as shown in Fig. 1. Fig. 1a displays a panoramic SEM image of the VO_2 (B) nanorods. As seen from the picture, the nanorods have regular shape with uniform diameters of about 100–300 nm width, and 1.0–2.5 μm length. The rods surface is smooth and flat, suggesting a complete growth of the nanorod under the present hydrothermal condition. The TEM image in Fig. 1b gives further support that individual VO_2 (B) nanorod with regular shapes. Furthermore, the high-resolution TEM (HRTEM) image of an individual nanorod, as shown in Fig. 1c, clearly exhibits the lattice fringe (upper-right inset in Fig. 1c), where the lattice planes with a spacing of 0.307 nm corresponding to the (0 0 2) planes, which is in a good mach with monoclinic VO_2 (B) (JCPDS No: 31-1438). The selected-area electron diffraction (SAED) patterns (bottom-left inset in Fig. 1c) further demonstrate the single-crystal character and well-defined crystalline degree of these nanorods. XRD patterns of the VO_2 (B) nanorods precursor are given in Fig. 1d. All the peaks can be well-

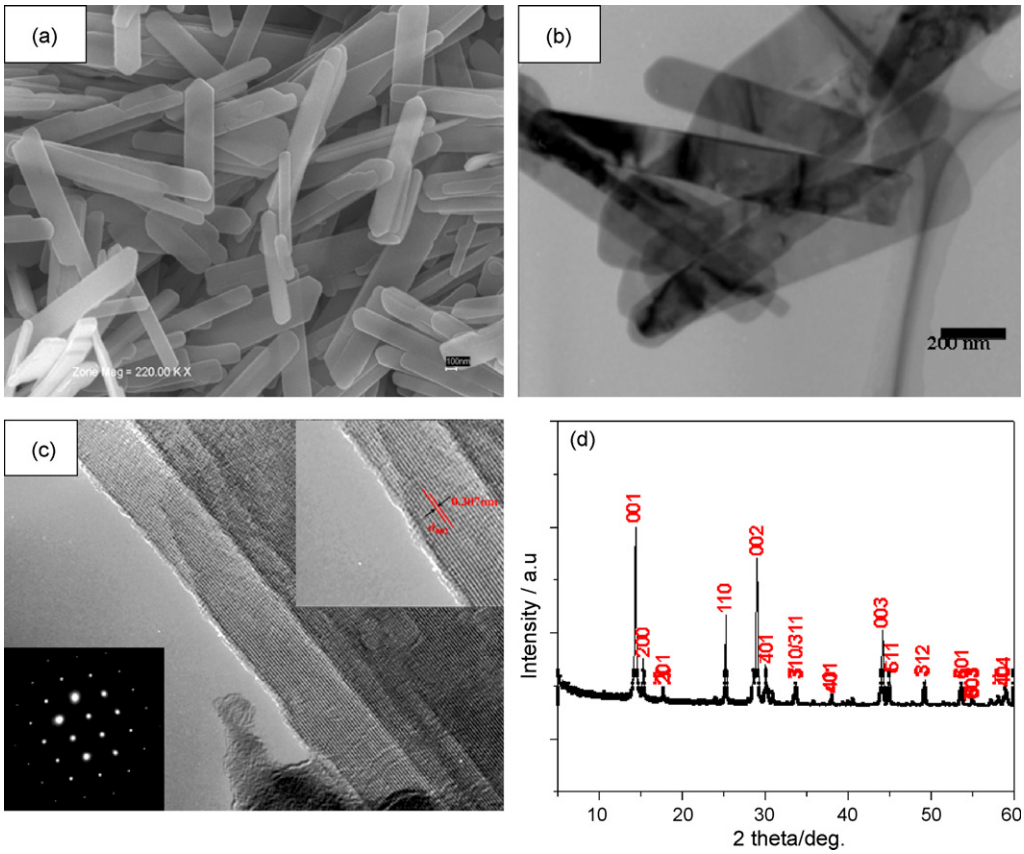

Fig. 1. Characterizations of VO_2 (B) nanorods precursor, (a) SEM image; (b) TEM image; (c) typical image of an individual VO_2 (B) nanorod and its SAED (lower-left inset) and lattice fringe (upper-right inset); (d) XRD patterns.

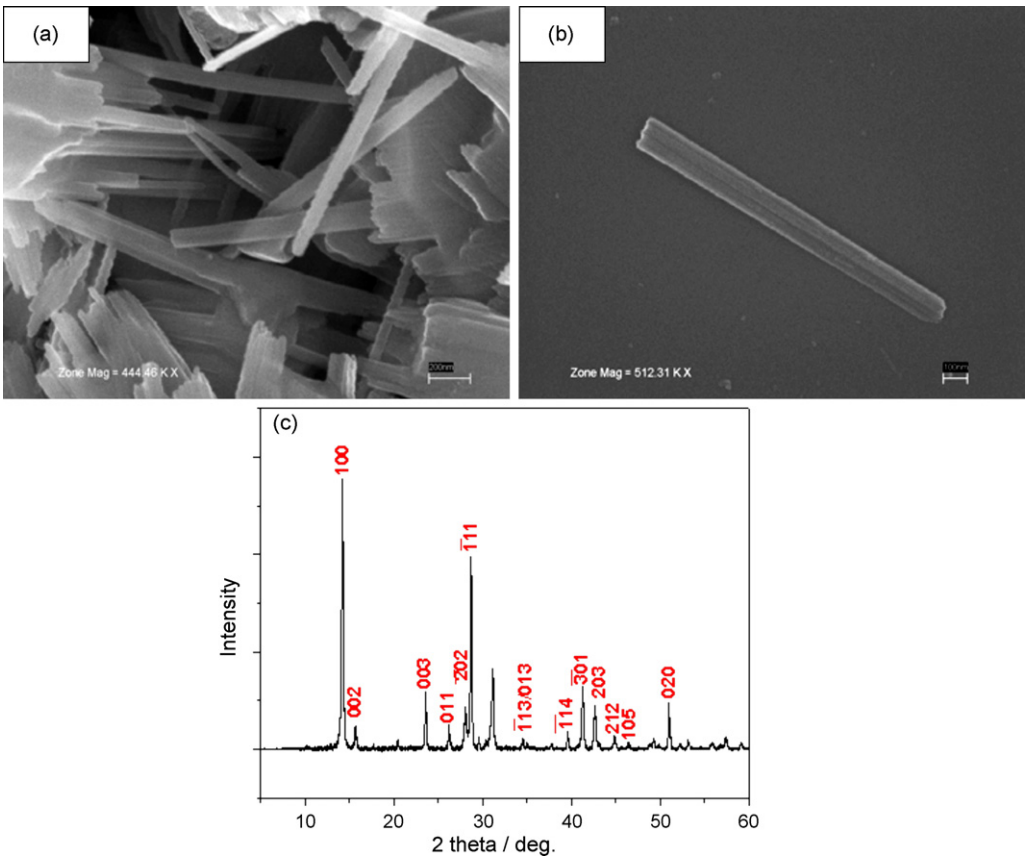

Fig. 2. SEM images of as-prepared LiV_3O_8 nanorods (a and b); XRD patterns of LiV_3O_8 nanorods (c).

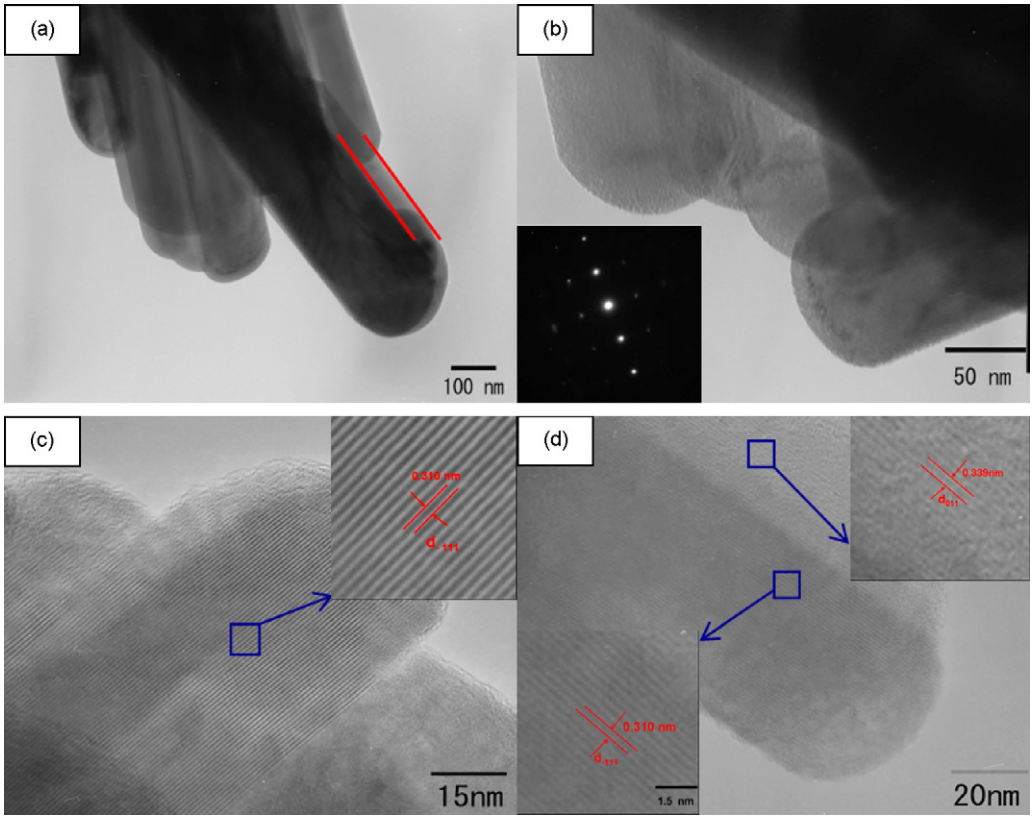

Fig. 3. TEM images and SAED of obtained LiV_3O_8 nanorods (a and b); high-resolution TEM images of typical LiV_3O_8 nanorods (c and d).

indexed to monolicnic VO_2 (B) phase (space group: *C2/m*, JCPDS No: 31-1438). It is interesting to note that the strongest peak set in Fig. 1d is (0 0 1), (0 0 2) and (0 0 3), which is quite different from that of the standard JCPDS data (JCPDS No: 31-1438), suggesting that the (0 0 *l*) planes are most probably the competitive growth direction in these nanorods. It should be noted that the XRD patterns give a good match to the HRTEM (upper-right inset in Fig. 1c), where the (0 0 2) planes are well-defined.

Fig. 2a depicts a panoramic SEM image of the as-synthesized LiV_3O_8 nanorods. As can be seen from the images, the LiV_3O_8 materials almost retain the precursor rods shape with 50–200 nm in width, and 1.0–2.0 μm in length. When we compare Fig. 2a with Fig. 1a, it is apparent that the LiV_3O_8 nanorods are somewhat more irregular in shape than that of the VO_2 (B) nanorods precursor. However, when taking into account of the preparation process of the LiV_3O_8, of which is come from the lithiation of VO_2 (B) nanorods, and subsequently calcinations at 450 °C for 10 h in air, it is reasonable that the crystal structure and the lattice parameters have changed, and there should have taken placed a rearrangement of the atoms. A typical SEM image of an individual LiV_3O_8 nanorod is displayed in Fig. 2b. As seen, the LiV_3O_8 material is almost maintains its straight nanorod-like configuration. The crystal structure of the LiV_3O_8 nanorods was analyzed by XRD and shown in Fig. 2c. All the diffraction peaks can be indexed to a pure monoclinic structure phase of space group *P21/m* LiV_3O_8 with the unit cell parameters of $a = 6.68$, $b = 3.596$, $c = 12.024$ Å, which was in agreement with the layered LiV_3O_8 (JCPDS No. 72-1193). The sharp and intense XRD peaks of the as-obtained LiV_3O_8 nanorods indicate its good degree of crystallinity.

A more detailed observation of the LiV_3O_8 nanorods was taken by TEM and HRTEM. Fig. 3a and b displays survey view of the as-synthesized LiV_3O_8 nanorods. Again, seen from the TEM images, the rods dimensions are hundreds nanometers in width, micrometers in length, moreover, the thickness is around several tens of nanometers (marked by red line in Fig. 3a), such an observation is in agreement with the SEM results. Moreover, the SAED patterns (inset in Fig. 3b) indicate these LiV_3O_8 nanorods are single-crystalline and well-defined in crystal phase. Furthermore, a typical LiV_3O_8 nanorod with smaller dimensions was carefully isolated and observed by HRTEM, shown in Fig. 3c and d. The face surface of the rods clearly exhibits a lattice planes with 0.310 nm spacing (inset in Fig. 3c, lower-left inset in Fig. 3d), corresponding to the spacing of $(\bar{1}\,1\,1)$ planes of monoclinic LiV_3O_8 (JCPDS No. 72-1193), and the lattice fringe in the side surface (upper-right inset in Fig. 3d) reveals its spacing of 0.339 nm, which is in a good match with the (0 1 1) planes of the monoclinic LiV_3O_8 phase. The LiV_3O_8 nanorods with of large size, such as the sample in Fig. 3a, are too thick to image under HRTEM, therefore only those rods with smaller dimensions are detected and observed by HRTEM, confirming their single-crystal character and highly crystalline structure. Although those LiV_3O_8 nanorods with of smaller sizes are not the total composition of the products, it still gives us some signatures of the as-prepared LiV_3O_8 nanorods, for instance, the well-defined crystal structure, and the growth direction of the LiV_3O_8 nanorods single-crystal in texture, and so on. It has been well-documented that nanostructured materials may facilitate the electrochemical intercalation/deintercalation of lithium ions among the host material, and the higher surface areas may provide more active sites, the specific BET surface areas of obtained LiV_3O_8 nanorods is 7.9 $m^2\,g^{-1}$; therefore, an improved electrochemical performance of the present LiV_3O_8 nanorods would be expected.

The typical cyclic voltammograms (CV) of the LiV_3O_8 nanorods are shown in Fig. 4a. The voltammograms were measured at a sweep rate of 0.5 mV s^{-1} in the potential range from 4.5 to 1.5 V vs. Li/Li^+ at room temperature. The main cathodic peaks appear at potential of about 3.4, 2.7 and 2.3 V vs. Li/Li^+ in the first cycle of the CV

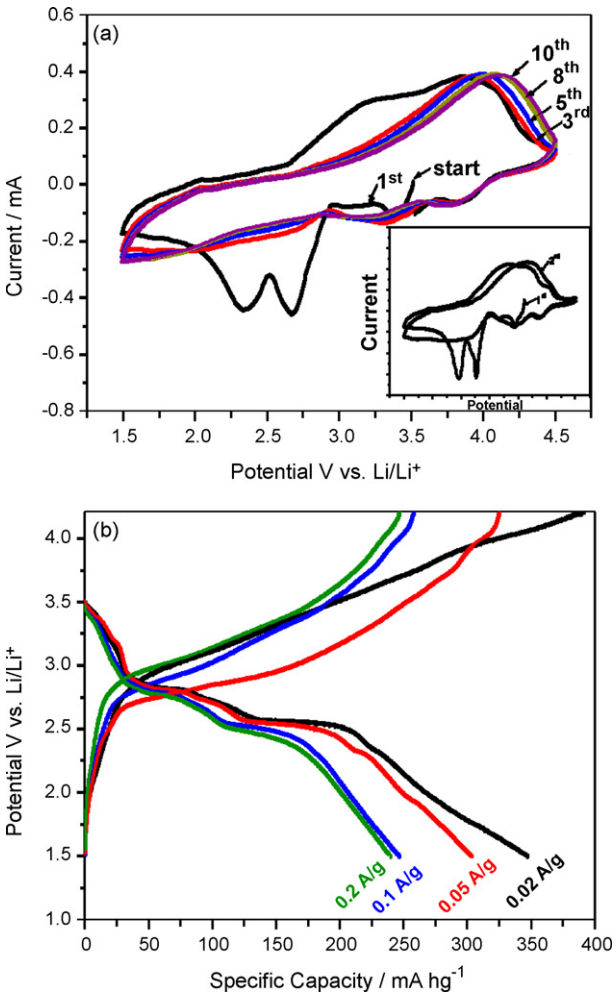

Fig. 4. (a) Cyclic voltammograms at scan rate of 0.5 mV s^{-1} (inset is the CV at 0.1 mV s^{-1} scan rate), and (b) first cycle of charge–discharge profiles at various current densities of single-crystal LiV_3O_8 nanorod. All the tests were worked in the potential window of 1.5–4.5 V (vs. Li/Li^+).

scans, which are ascribed to lithium insertion process for LiV_3O_8. This process simultaneously induces several phase transformations between couples of $Li_{1+x}V_3O_8$ ($x = 0.1$–4) [22,23]. It is apparent that the first voltammograms are quite different from the rest scans, indicating some unexpected structural modification has probably taken place during the first CV scans, it is further confirmed by slower scan at 0.1 mV s^{-1} (inset in Fig. 4a). As can be seen, the shape of first scan at 0.1 mV s^{-1} is same as that of at 0.5 mV s^{-1}, and different from those of following scans, it is thus believed that such a behavior is its intrinsic property of present LiV_3O_8 nanorods. However, in the subsequent prolonged cycling till to 10th cycle, the curves are nearly identical in shape, implying a good reversibility. The galvanostatic first cycle of charge–discharge behaviors of the LiV_3O_8 nanorods recorded over the potential range between 1.5 and 4.5 V vs. Li/Li^+ at various current densities from 0.05 to 0.5*C* (where *C* corresponds to the complete discharge in 1 h) are shown in Fig. 4b. The discharge capacity of the prepared LiV_3O_8 nanorods is 348 mAh g^{-1} at a current density of 0.02 A g^{-1}, corresponding to 3.7Li being intercalated to the LiV_3O_8 material, and it still delivers a capacity of 239 mAh g^{-1} (about 2.5Li) at the current density of 0.2 A g^{-1}, implying its good rate capacity of the present LiV_3O_8 nanorods. Furthermore, it is worthwhile to be noted that at 0.02 and 0.05 A g^{-1} current densities, there are three apparent discharge plateaus at 2.85, 2.6 and 2.3 V, whereas at 0.1 and 0.2 A g^{-1} current densities, there are only two patent plateaus located at 2.85

and 2.6 V. It has been reported that the discharge plateau of 2.8 V is an electrochemical signature of single-phase insertion process [23,24], and the 2.6 V plateau is a signature of the two-phase transformation between $Li_{1+x}V_3O_8$ ($1 \le x \le 2$) and $Li_4V_3O_8$, [23] while the last 2.3 V process at lower current densities of 0.02 and 0.05 A g^{-1}, it concerns a slower kinetic insertion process [25–27]. Actually, this 2.3 V insertion process was also regarded as one of the main reasons that induced the capacity fading in the following cell operations, because it was tentatively explained that some reactivity with the electrolyte of $Li_4V_3O_8$ phase maybe occurred [23]. In other words, it was suspected that some reactions between electrolyte and $Li_4V_3O_8$ phase had occurred, leading to either a passive film formation or materials dissolution, in the case of the contact time of electrode materials with electrolyte was long enough. However, in our case, the LiV_3O_8 nanorods surprisingly exhibit a good cycling performance even under the lower current densities of 0.02 and 0.05 A g^{-1}.

The cycling performance is another important parameter for an electrode material. Thereby, the cycling behaviors of the present LiV_3O_8 nanorods were investigated at various current densities between 4.5 and 1.5 V vs. Li/Li^+. Fig. 5A displays the specific discharge capacities as a function of the cycle number, at the current densities from 0.02 (about *C*/20) to 0.1 A g^{-1} (about *C*/4). When this material is cycled at 0.02 A g^{-1} (curve a), it exhibits a rather high capacity for lithium; after 15 cycles, the specific capacity is still maintaining 382 mAh g^{-1}. The material cycled at 0.05 (curve b) and 0.1 A g^{-1} (curve c) also exhibits good capacity cycling, the former is stabilized at around 315 mAh g^{-1} till 50 cycles, and the latter is

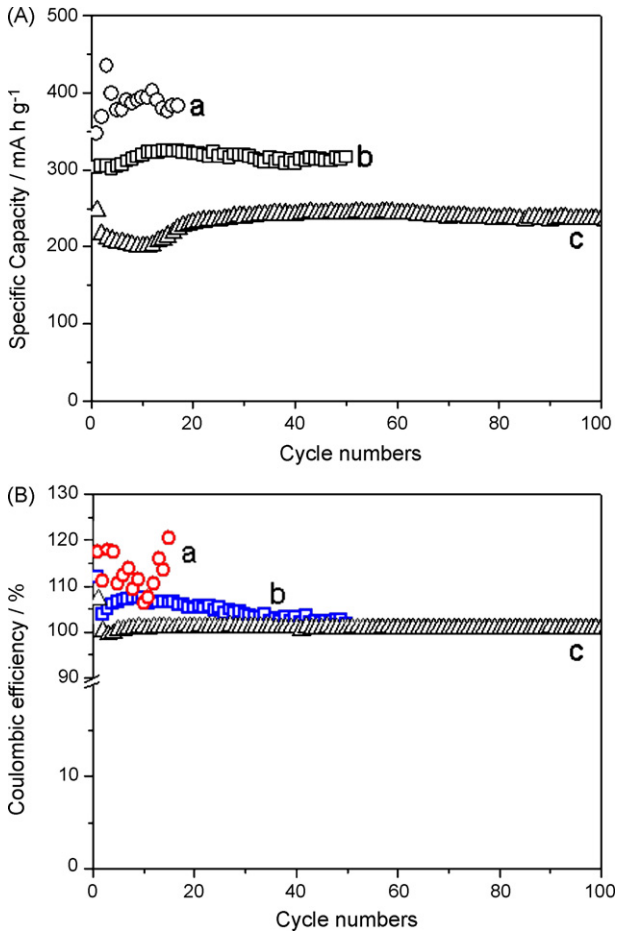

Fig. 5. The specific capacities (A) and coulombic efficiency (B) as a function of the cycling numbers at various current densities of 0.02 A g^{-1} (curve a), 0.05 A g^{-1} (curve b) and 0.1 A g^{-1} (curve c).

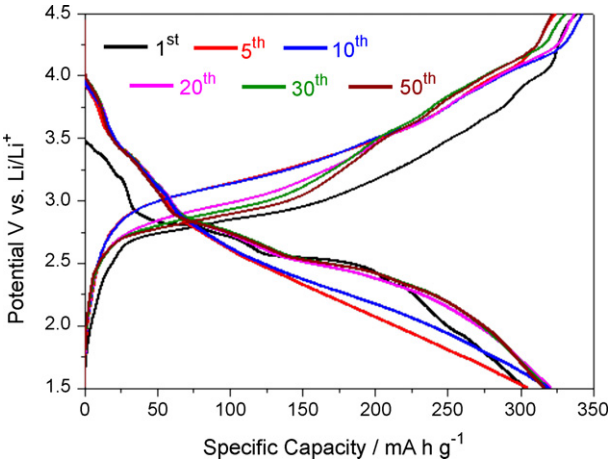

Fig. 6. The different cycles of charge–discharge profiles at a current density of 0.05 A g^{-1}.

kept at about 236 mA h g^{-1} till 100 cycles, to our best knowledge, it is one of the most stable and highest values for LiV_3O_8 material, that have ever been reported to date [28–33]. Furthermore, as can been seen, the material displays an excellent capacity retention in a long-term range. When cycled at 0.05 A g^{-1} (curve b), which corresponds to a discharge rate of *C*/8, it does not show any capacity fading until 50 cycles. When cycled at 0.1 A g^{-1} (curve c), although there is an obvious capacity fading in the first 10 cycles, it still retains as high as 96% of its initial capacity till 100 cycles, in other words, the average capacity loss of LiV_3O_8 nanorods is about 0.1 mAh g^{-1} per cycle during 100 charge–discharge cycles. The excellent cycling ability of the present LiV_3O_8 nanorods electrode could be probably attributed to its high crystallinity as confirmed by XRD patterns (Fig. 2c) and TEM together with HRTEM (Fig. 3b–d). The higher crystalline degree would improve the stability of the crystallographic structure of the LiV_3O_8 nanorods during the lithium insertion/extraction among the host material. The coulombic efficiency (calculated from the charge capacity/discharge capacity of every cycle) vs. cycle numbers at various current densities is displayed in Fig. 5B. The scattering of the coulombic efficiency and greater than 100% at 0.02 A g^{-1} (curve a) may be explained by either the passive film formation and electrode materials dissolution, or electrolyte decomposition, as mentioned earlier, when the current density is low and induced by long-time contact between the electrode materials with electrolyte. However, when cycled at 0.05 A g^{-1} to 50 cycles (curve b) and 0.1 A g^{-1} to 100 cycles (curve c), the coulombic efficiencies stabilize at about 100%, implying its good reversibility during the long-term charge/discharge tests when cycled at a moderate current density of 0.05 and 0.1 A g^{-1}.

Finally, it should be pointed out that although the present LiV_3O_8 nanorods exhibit excellent cycling ability at various current densities, it is also noticeable that the shape of the charge–discharge profile of the first cycle with rest cycles is different. Fig. 6 displays the different cycles of charge–discharge profiles at the current density of 0.05 A g^{-1}. It is apparent that there are several discharge patent plateaus during the first cycle of discharge, which corresponds to the phase transition between the couples of $Li_{1+x}V_3O_8$ (x = 0.1–4), however, except the first cycle, the rest cycles till to 50 cycles, there are no any obvious discharge plateau, suggesting there should have taken place some irreversible reactions during the first charge–discharge process, this phenomenon has also been noticed in the CV scans (Fig. 4a). A definite explanation for this phenomenon is unavailable in present stage, clearly, further investigations on the structural evolution upon cycling are required and

the relative work is on the going way. However, it should be noted that the aforementioned difference between the first cycle with other cycles does not bring about a negative influence on the electrochemical properties of the LiV_3O_8 nanorods material, and the charge–discharge curves are kept almost identical during the following cycling tests, indicating its good reversibility of the lithium intercalation/deintercalation.

It is generally accepted in the field of lithium-ion batteries that the nano-scaled materials with shorter transport pathway could inevitably lead to more efficient lithium insertion and less volume change upon lithium extraction [18–20,33], which should improve not only the discharge capacity but also the capacity retention over charge–discharge cycling tests. Furthermore, as mentioned in Section 1, the electrochemical properties of the LiV_3O_8 cathode material are greatly depended on not only the preparation methods but also the morphology and texture of the materials. In this work, the single-crystalline LiV_3O_8 nanorods with nano-scaled dimensions, the dominant dimensions of which are hundreds nanometers in width, and the thickness is around several tens of nanometers, together with highly crystalline degree would probably facilitate the transport of the lithium ions, and less collapse of the crystal structures upon lithium removal. On the other hand, it was reported that the surface areas of the electrode materials always play an important and direct role on the electrochemical performance [33,34]. The larger of the surface areas of the materials, the more active contact sites between electrolyte and electrode materials, which is beneficial to faster diffusion of the lithium ions and decreased polarization [34,35]. The surface areas of present LiV_3O_8 nanorods of 7.9 $m^2\,g^{-1}$, higher than those of reported [22,32–34], would be another effective key for the improved electrochemical properties of the LiV_3O_8 nanorods.

In summary, we have employed a home-made VO_2 (B) nanorods as the vanadium precursor to prepare the LiV_3O_8 cathode material. The as-obtained single-crystalline LiV_3O_8 nanorods with high crystallinity greatly improved the stability of the crystallographic structure during cycling. Furthermore, this material exhibited as high as 382 mAh g^{-1} (about 4Li) discharge capacity till 15 cycles recorded at 0.02 A g^{-1}; and still delivered 315 mAh g^{-1} after 50 cycles at the current density of 0.05 A g^{-1}. Moreover, it also displays an excellent long-term cyclability when cycled at 0.1 A g^{-1}, because the capacity retention is nearly kept at 96% even after 100 cycles. Based on above experimental results, we believe that such a LiV_3O_8 material would be of very interesting candidate material for the next generation rechargeable lithium batteries.

Acknowledgement

The authors thank M. Ichihara at The University of Tokyo for his kindly help with the TEM observations, and also acknowledge the financial support from Li-EAD project of New Energy and Industrial Technology Development Organization (NEDO).

References

[1] K. West, Z. Bachau-C, S. Skaarup, Y. Saidi, J. Barker, I.I. Olsen, R. Pynenburg, R. Koksbang, J. Electrochem. Soc. 143 (1996) 820.
[2] N. Kumagai, A. Yu, J. Electrochem. Soc. 144 (1997) 830.
[3] J.O. Besenhard, R. Schöllhorn, J. Power Source 1 (1976) 267.
[4] S. Panero, M. Pasquali, G. Pistoia, J. Electrochem. Soc. 130 (1983) 1226.
[5] K. Nassau, D.W. Murphy, J. Non-Cryst. Solids 44 (1981) 297.
[6] A. Yu, N. Kumagai, Z. Liu, J.Y. Lee, J. Power Source 74 (1998) 117.
[7] G. Pistoia, M. Pasquali, M. Tocci, R.V. Moshtev, V. Manev, J. Electrochem. Soc. 132 (1985) 281.
[8] G. Pistoia, M. Pasquali, G. Wang, L. Li, J. Electrochem. Soc. 137 (1990) 2365.
[9] M. Pasquali, G. Pistoia, Electrochim. Acta 36 (1991) 1549.
[10] G. Pistoia, G. Wang, D. Zane, Solid State Ionics 76 (1995) 285.
[11] H. Ma, S. Zhang, W. Ji, Z. Tao, J. Chen, J. Am. Chem. Soc. 130 (2008) 5361.
[12] B.S. Guiton, Q. Gu, A.L. Prieto, M.S. Gudiksen, H. Park, J. Am. Chem. Soc. 127 (2005) 498.
[13] A.R. Armstrong, G. Armstrong, J. Canales, R. Garcia, P.G. Bruce, Adv. Mater. 16 (2006) 1133.
[14] Y. Wang, G. Cao, Chem. Mater. 18 (2006) 2787.
[15] X. Li, F. Cheng, B. Guo, J. Chen, J. Phys. Chem. B 109 (2005) 14017.
[16] X. Li, X. Chen, X. Chen, C. Han, C. Shi, J. Crystal Growth 309 (2007) 43.
[17] J.Y. Luo, H.M. Xiong, Y.Y. Xia, J. Phys. Chem. C 112 (2008) 12051.
[18] Y. Gu, D. Chen, X. Jiao, F. Liu, J. Mater. Chem. 16 (2006) 4361.
[19] X.W. Lou, D. Deng, J.Y. Lee, J. Feng, L.A. Archer, Adv. Mater. 20 (2008) 258.
[20] K.M. Shaju, F. Jiao, A. Debart, P.G. Bruce, Phys. Chem. Chem. Phys. 9 (2007) 1837.
[21] X. Liu, J. Wang, J. Zhang, S. Yang, J. Mater. Sci. 42 (2007) 867.
[22] S. Jouanneau, A. Salle, A. Verbaere, M. Deschamps, S. Lascaud, D. Guyomard, J. Mater. Chem. 13 (2003) 921.
[23] S. Jouanneau, A. Salle, A. Verbaere, D. Guyomard, J. Electrochem. Soc. 152 (2005) A1660.
[24] D. Djurado, M. Barral, Y. Chabre, J.E. Fisher, in: P. Bernier (Ed.), Chemical Physics of Intercalation II, Plenum Press, New York, 1993, p 255.
[25] J. Kawakita, T. Miura, T. Kishi, J. Power Source 83 (1999) 79.
[26] J. Kawakita, T. Miura, T. Kishi, Solid State Ionics 120 (1999) 109.
[27] J. Kawakita, Y. Katayama, T. Miura, T. Kishi, Solid State Ionics 107 (1998) 145.
[28] S.Y. Chew, C. Feng, S.H. Ng, J. Wang, Z. Guo, H. Liu, J. Electrochem. Soc. 154 (2007) A633.
[29] T.J. Patey, S.H. Ng, R. Büchel, N. Tran, F. Krumeich, J. Wang, H. Liu, P. Novák, Electrochem. Solid-State Lett. 11 (2008) A46.
[30] N. Tran, G. Bramnik, H. Hibst, J. Prölβ, N. Mronga, M. Holzapfel, W. Scheifele, P. Novák, J. Electrochem. Soc. 155 (2008) A384.
[31] A.M. Kannan, A. Manthiram, J. Power Source 159 (2006) 1405.
[32] S. Jouanneau, A. Verbaere, S. Lascaud, D. Guyomard, Solid State Ionics 177 (2006) 311.
[33] G. Yang, G. Wang, W. Hou, J. Phys. Chem. B 109 (2005) 11186.
[34] V. Subramanian, C.L. Chen, H.S. Chou, G.T.K. Fey, J. Mater. Chem. 11 (2001) 3348.
[35] H.S. Zhou, D.L. Li, M. Hibino, I. Honma, Angew. Chem. Int. Ed. 44 (2005) 797.